



# Dynamic response of biofilm microbial ecology to *para*-chloronitrobenzene biodegradation in a hydrogen-based, denitrifying and sulfate-reducing membrane biofilm reactor

Haixiang Li <sup>a,1</sup>, Lijie Zhou <sup>b,1</sup>, Hua Lin <sup>a</sup>, Xiaoyin Xu <sup>c</sup>, Renyong Jia <sup>d</sup>, Siqing Xia <sup>c,\*</sup>

<sup>a</sup> Guangxi Key Laboratory of Environmental Pollution Control Theory and Technology, Guilin University of Technology, Guilin, Guangxi 541004, PR China

<sup>b</sup> College of Chemistry and Environmental Engineering, Shenzhen University, Shenzhen 518060, PR China

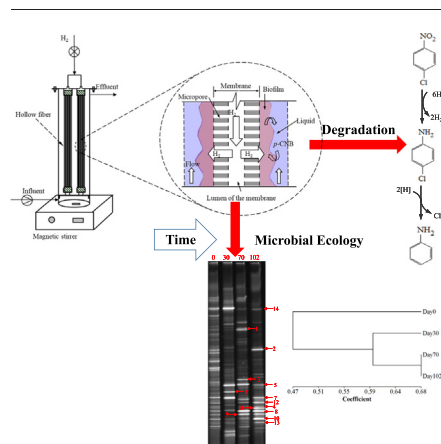
<sup>c</sup> State Key Laboratory of Pollution Control and Resource Reuse, College of Environmental Science and Engineering, Tongji University, Shanghai 200092, PR China

<sup>d</sup> Shanghai Urban Construction Design and Research Institute, Shanghai 200125, China

## HIGHLIGHTS

- Nitrate and sulfate reduction competed more strongly for hydrogen than *p*-CNB.
- Presence of *p*-CNB had a more advantageous effect on biofilm microbial community.
- *Pseudomonas* played a significant role in *p*-CNB biotransformation.

## GRAPHICAL ABSTRACT



## ARTICLE INFO

### Article history:

Received 11 March 2018

Received in revised form 19 June 2018

Accepted 19 June 2018

Available online xxxx

Editor: Zhen (Jason) He

### Keywords:

Hydrogen-based, denitrifying and sulfate-reducing membrane biofilm reactor (MBfR)  
*para*-chloronitrobenzene  
Biofilm microbial ecology

## ABSTRACT

The dynamic response of biofilm microbial ecology to *para*-chloronitrobenzene (*p*-CNB) biodegradation was systematically evaluated according to the composition and loading of electron acceptors and H<sub>2</sub> availability (controlled by H<sub>2</sub> pressure) in a hydrogen-based, denitrifying and sulfate-reducing membrane biofilm reactor (MBfR). To accomplish this, a laboratory-scale MBfR was set up and operated with different influent *p*-CNB concentrations (0, 2, and 5 mg *p*-CNB/L) and H<sub>2</sub> pressures (0.04 and 0.05 MPa). Polymerase chain reaction-denaturing gel electrophoresis (PCR-DGGE) and cloning were then applied to investigate the bacterial diversity response of biofilm during *p*-CNB biodegradation. The results showed that denitrification and sulfate reduction largely controlled the total demand for H<sub>2</sub>. Additionally, the DGGE fingerprint demonstrated that the addition of *p*-CNB, which acted as an electron acceptor, was a critical factor in the dynamics of the MBfR biofilm microbial ecology. The presence of *p*-CNB also had a more advantageous effect on the biofilm microbial community. Additionally, clone library analysis showed that *Proteobacteria* (especially *beta*- and *gamma*-) comprised the majority of the microbial biofilm response to *p*-CNB biodegradation,

\* Corresponding author.

E-mail address: [siqingxia@tongji.edu.cn](mailto:siqingxia@tongji.edu.cn) (S. Xia).

<sup>1</sup> Haixiang Li and Lijie Zhou contributed equally to this study.

and that *Pseudomonas* sp. (*Gammaproteobacteria*) played a significant role in the biotransformation of *p*-CNB to aniline.

© 2018 Elsevier B.V. All rights reserved.

## 1. Introduction

As an important raw material for the synthesis of dyes, medicines, pesticides, resins, and preservatives, chloronitrobenzenes (CNB) has been widely applied worldwide, especially in China (Le et al., 2011b; Wu et al., 2017). Chloronitrobenzenes contain *ortho*-chloronitrobenzene (*o*-CNB), *meta*-chloronitrobenzene (*m*-CNB), and *para*-chloronitrobenzene (*p*-CNB), among which *p*-CNB has the highest biological toxicity and risk. Previous studies (Hong et al., 2002; Matsumoto et al., 2006) have shown that *p*-CNB has toxic effects on algae, fish, aquatic plants, and especially humans, and that it is considered a mutagenic and carcinogenic organic contaminant. *p*-CNB has been found at 0.005–3.7 mg/L in lakes and rivers close to industrial factories in China (Huang et al., 2016; Li et al., 2014); thus, the threat that *p*-CNB poses to drinking water in the region, especially ground water, is of high interest.

The benzene of *p*-CNB contains two strong electron-withdrawing groups (nitro and chloro substituents), and anaerobic microbial reduction is considered an important pathway for *p*-CNB biodegradation (Huang et al., 2016; Le et al., 2011a) because the microbial attack is easily conducted in the presence of electron donors. Previous studies have shown that a variety of microorganisms can transform chloronitrobenzenes via nitro reduction and reductive dechlorination under anaerobic conditions, such as *Pseudomonas* (Park et al., 1999), *Rhodococcus* (Park et al., 1999), *Comamonas* (Wu et al., 2006), *Sphingomonas* (Zhang et al., 2013), and *Burkholderia* (Zhang et al., 2013) species. High levels of nitrate and sulfate, which are common oxidized contaminants, are often found in surface water or groundwater. Moreover, denitrifying bacteria (DB) and sulfate reducing bacteria (SRB) are widely distributed in aquatic environments. Most of the bacteria mentioned above, including *Pseudomonas*, *Rhodococcus*, and *Comamonas*, also belong to DB and/or SRB (Zhang et al., 2010; Su et al., 2012; Chen et al., 2012; Wu et al., 2015).

Several organic or inorganic compounds can be used as electron donors for anaerobic microbial reduction of chloronitrobenzenes. Hydrogen gas is considered as a clean, non-toxic, residue-free, and inexpensive inorganic electron donor that can be used in place of other organic compounds. Zhu et al. (2012) found that H<sub>2</sub>, working as an electron donor, greatly enhanced *p*-CNB biodegradation in an anaerobic digestion system with ZVI, and ultimately reduced the operational costs of *p*-CNB removal. As a new technology for the bioreduction of oxidized contaminants, hydrogen-based membrane biofilm reactor (MBfR) deliver H<sub>2</sub> directly via molecular diffusion through the wall of a bubble-less gas-transfer membrane (Aydin et al., 2016; Chen et al., 2017; Zhang et al., 2016). Autotrophic bacteria that live as a biofilm on the outer surface of the membrane then oxidize H<sub>2</sub> to reduce one or several electron acceptors in the water (Xia et al., 2016). Thus, MBfR provides an effective mechanism for removing *p*-CNB from water via bioreduction. Previous studies (Li et al., 2014; Xia et al., 2011) have shown the excellent performance of MBfR for *p*-CNB biodegradation. However, during MBfR operation, time is required to culture bacteria in the biofilm to levels capable of highly-effective *p*-CNB biodegradation. Many studies have reported that the operational conditions, such as electron acceptor composition and loading and electron donor availability (H<sub>2</sub> pressure), influence the microbial community in MBfRs (Zhou et al., 2014; Ontiveros-Valencia et al., 2017). Moreover, nitrate and sulfate, which are common electron acceptors, can be reduced simultaneously and often have various effects on the reduction of other electron acceptors in MBfRs (Chung et al., 2006; Chung et al., 2008; Lai

et al., 2014; Chen et al., 2017). The interactions between nitrate, sulfate, and other electron acceptors also depend on the microbial community structure. Therefore, under the conditions of co-reduction of nitrate and sulfate, determining methods for the acceleration of the enrichment of *p*-CNB-reducing bacteria is one of the key hurdles that must be overcome to enable the widespread application of MBfR for *p*-CNB degradation.

To conduct a systematic evaluation of the biofilm microbial community exposed to different electron acceptors, we first developed a biofilm community capable of reducing nitrate and sulfate. We then investigated whether the biofilm populated with DB and/or SRB could induce *p*-CNB reduction. Next, we modified the *p*-CNB loading and H<sub>2</sub> availability by varying the influent *p*-CNB concentration and H<sub>2</sub> pressure. The response of bacterial diversity in the biofilm to MBfR reaction was subsequently investigated by PCR-DGGE and a cloning library.

## 2. Materials and methods

### 2.1. Experimental set of the MBfR

Fig. 1a presents the schematic of the laboratory-scale MBfR used in the present study, and Fig. 1b shows the longitudinal cross-section of the hollow fiber membranes installed in the modules of the reactor. A magnetic stirrer was applied to generate stirring power to mix the liquid in the MBfR completely. The reactor was 22 cm in height and 7 cm in inner diameter, with a total available volume of 750 mL, including 125 cm<sup>3</sup> of two hollow fiber membrane modules (made of polyvinyl chloride with a pore size of 0.01 μm; Litree Company, Suzhou, China). These membrane modules were directly submerged in the bulk fluid and easily disassembled from the reactor for membrane rinsing or repairing. Each membrane module contained 66 hollow fibers with outer and inner diameters of the fiber of 0.15 cm and 0.085 cm, respectively, that provided a 495 cm<sup>2</sup> surface area. The hollow fibers contained a single hydrophobic layer structure that served as the means for bubble-less H<sub>2</sub> delivery via diffusion. In addition, a single peristaltic pump (Longer BT50-1J, Baoding, China) was used to keep a feed rate of 2.0 mL/min. Finally, pure H<sub>2</sub> gas was supplied to the inside of hollow fibers through a H<sub>2</sub> gas tank via a partial pressure valve.

MBfR was seeded with bacteria obtained from another laboratory-scale MBfR that had been treated with nitrate for over 3 months. Specifically, the MBfR was operated with different influent *p*-CNB concentrations (0, 2, and 5 mg/L) and H<sub>2</sub> pressures (0.04 and 0.05 MPa) as shown in Table 1. The MBfR was operated under the Phase 1 conditions (Table 1) to achieve stable effluent performance, after which the experiments were started. The MBfR achieved three steady states (Phase 1, Phase 2, and Phase 3) over 100 days.

### 2.2. Synthetic media

The composition of the MBfR feed medium was (mg/L): KH<sub>2</sub>PO<sub>4</sub> (128), Na<sub>2</sub>HPO<sub>4</sub> (434), MgSO<sub>4</sub>·7H<sub>2</sub>O (200), CaCl<sub>2</sub>·2H<sub>2</sub>O (1), FeSO<sub>4</sub>·7H<sub>2</sub>O (1), NaHCO<sub>3</sub> (252), NaNO<sub>3</sub> (30), ZnSO<sub>4</sub>·7H<sub>2</sub>O (0.013), MnCl<sub>2</sub>·4H<sub>2</sub>O (0.004), H<sub>3</sub>BO<sub>3</sub> (0.038), CoCl<sub>2</sub>·6H<sub>2</sub>O (0.025), CuCl<sub>2</sub>·2H<sub>2</sub>O (0.001), NiCl<sub>2</sub>·6H<sub>2</sub>O (0.001), Na<sub>2</sub>MoO<sub>4</sub>·2H<sub>2</sub>O (0.004), and Na<sub>2</sub>SeO<sub>3</sub> (0.004). The culture medium was prepared in a 10.0 L (available volume) brown glass bottle that had been purged with nitrogen gas to eliminate dissolved oxygen. NaNO<sub>3</sub> and NaHCO<sub>3</sub> were used as the inorganic nitrogen and carbon sources for the growth of autotrophic microorganisms, respectively. Phosphate buffer (KH<sub>2</sub>PO<sub>4</sub> + Na<sub>2</sub>HPO<sub>4</sub>) was

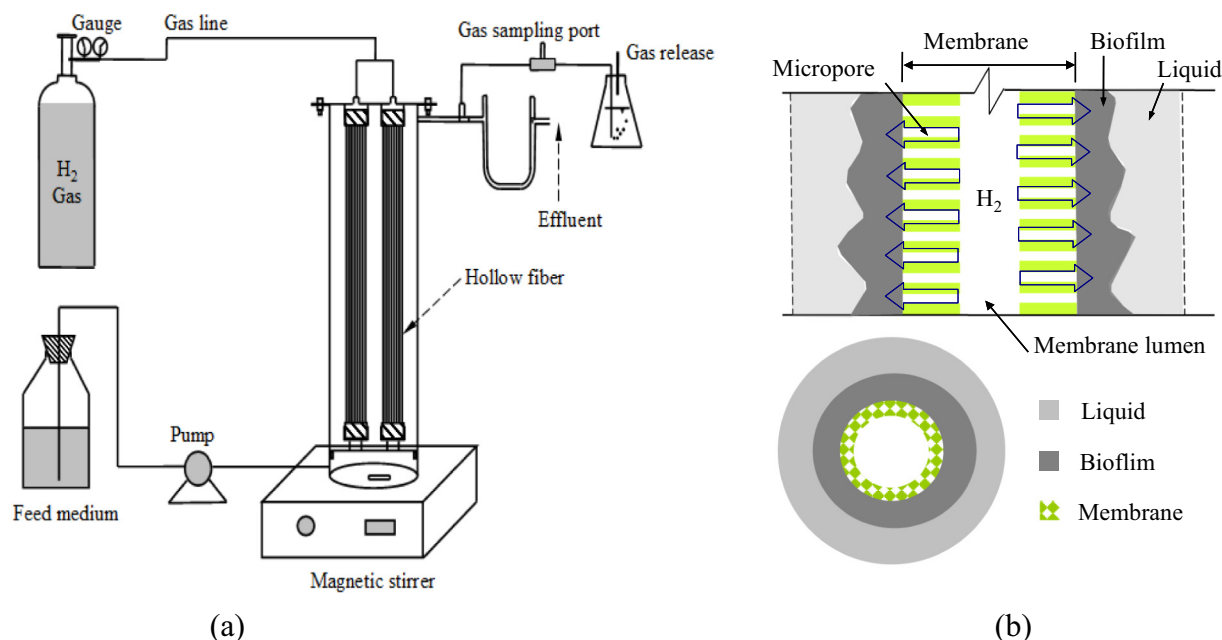


Fig. 1. (a) Schematic of membrane biofilm reactor and (b) longitudinal cross-section of a hollow fiber membrane.

used to keep the initial pH of the influent around 7.5 and to prevent a sharp rise in pH during the reduction process.

### 2.3. Biofilm sampling

Biofilm samples were collected at the end of each steady phase (on Day 30, 70 and 102, respectively). For each collection, 3 hollow fibers (10 cm length in term of fiber) were first cut from different locations on the membrane modules and then combined into a composite sample. The hollow fiber membranes were then cut into short pieces of approximately 1.0 cm, after which the biofilms were detached from the membranes using an ultrasonic instrument (SK3300–35 KHz, China). Biofilm samples were subsequently washed in TENP buffer, then re-

suspended in sodium phosphate buffer before DNA extraction (Xu et al., 2015).

### 2.4. DNA extraction and PCR amplification

Total genomic DNA was extracted from biofilm samples using a Fast DNA Spin Kit (EZ-10, Bio Basic Inc., Canada) according to the manufacturer's instructions. Successful extraction was confirmed by gel electrophoresis, after which DNA was stored at  $-20^{\circ}\text{C}$  until further processing. The 16S rRNA genes were amplified from the DNA extracts by PCR using a thermal cycler (Thermo PXE 0.2, USA) with the following steps: initial denaturation at  $94^{\circ}\text{C}$  for 5 min followed by 30 cycles of  $94^{\circ}\text{C}$  for 45 s (denaturation),  $55^{\circ}\text{C}$  for 1 min (annealing), and  $72^{\circ}\text{C}$  for 90 s (extension), and then a final extension at  $72^{\circ}\text{C}$  for 7 min, after which the

Table 1  
Water quality parameters and operational conditions during each steady state.

|   | Phase 1          | Phase 2                         | Phase 3                         |
|---|------------------|---------------------------------|---------------------------------|
| Dates (days)  | 26–30            | 65–70                           | 98–102                          |
| Electron acceptors  | Nitrate, sulfate | <i>p</i> -CNB, nitrate, sulfate | <i>p</i> -CNB, nitrate, sulfate |
| H <sub>2</sub> pressure (MPa)                                     | 0.04             | 0.04                            | 0.05                            |
| HRT (h)   | 5.2              | 5.2                             | 5.2                             |
| Influent nitrate (mg/L)   | 10               | 10                              | 10                              |
| Influent sulfate (mg/L)   | 55               | 55                              | 55                              |
| Influent <i>p</i> -CNB (mg/L)                                     | –                | 2                               | 5                               |
| Average effluent <i>p</i> -CNB ( $\mu\text{g/L}$ )                | –                | $90 \pm 23$                     | $1827 \pm 139$                  |
| Average effluent <i>p</i> -CAN ( $\mu\text{g/L}$ )                | –                | $50 \pm 15$                     | $99 \pm 14$                     |
| Average effluent aniline ( $\mu\text{g/L}$ )                      | –                | $211 \pm 32$                    | $342 \pm 13$                    |
| Removal of nitrate  | 80.9%            | 90.7%                           | 90%                             |
| Removal of sulfate  | 10.9%            | 18.2%                           | 40.0%                           |
| Removal of <i>p</i> -CNB  | –                | 95.5%                           | 63.6%                           |
| Nitrate flux ( $\text{g N/m}^2 \cdot \text{d}$ )                  | 0.233            | 0.243                           | 0.244                           |
| Sulfate flux ( $\text{g SO}_4^{2-}/\text{m}^2 \cdot \text{d}$ )   | 0.262            | 0.291                           | 0.640                           |
| <i>p</i> -CNB flux ( $\text{g p-CNB/m}^2 \cdot \text{d}$ )        | –                | 0.055                           | 0.097                           |
| Electron-nitrate flux ( $\text{eq/m}^2 \cdot \text{d}$ )          | 0.0832           | 0.0868                          | 0.0871                          |
| Electron-sulfate flux ( $\text{eq/m}^2 \cdot \text{d}$ )          | 0.0218           | 0.0243                          | 0.0533                          |
| Electron- <i>p</i> -CNB flux ( $\text{eq/m}^2 \cdot \text{d}$ )   | –                | 0.0028                          | 0.0049                          |
| Distribution of electron-nitrate flux                             | 79.2%            | 76.2%                           | 59.9%                           |
| Distribution of electron-sulfate flux                             | 20.8%            | 21.3%                           | 36.7%                           |
| Distribution of electron- <i>p</i> -CNB flux                      | –                | 2.5%                            | 3.4%                            |
| Average effluent H <sub>2</sub> concentration ( $\mu\text{g/L}$ ) | 351              | 185                             | 87                              |
| H <sub>2</sub> flux ( $\text{g/m}^2 \cdot \text{d}$ )             | 0.097            | 0.117                           | 0.143                           |
| H <sub>2</sub> utilization efficiency                             | 89.4%            | 95.4%                           | 98.2%                           |

samples were held at 4 °C. The universal primers used for bacterial gene amplification were 27F and 1492R (Xu et al., 2015). In one PCR reaction (50 µL), the following reactants were added: 1× PCR buffer, 2 mmol/L MgCl<sub>2</sub>, 0.2 mmol/L dNTP, 0.5 mmol/L of each primer, 1.25 unit of *Taq* polymerase, and 40 ng of DNA template.

### 2.5. DGGE analysis

For more sensitive DGGE analysis, nested PCR of the above PCR products was conducted using the primers 357F-GC and 518R (Xia et al., 2010). The amplification program was predenaturation at 94 °C for 5 min followed by 32 cycles of 94 °C for 45 s, 57 °C for 1 min, and 72 °C for 90 s and then final extension at 72 °C for 7 min. Amplification products were separated by 8% (w/v) polyacrylamide gel containing denatured gradients (urea and formamide) at 35%–55% using a D-code DGGE System (BioRad, USA). Electrophoresis was conducted using a 1 × TAE buffer at 120 V and 60 °C for 8 h. After electrophoresis, the gel was stained with SDNA-Nucleic Acids Stain Dye (Bio Basic Inc., Canada), after which it was washed with sterile water and scanned with an UV transilluminator (FR-980A, Furi Tech. Ltd., Shanghai, China). Specific DGGE bands were then manually excised from the gel, re-amplified, cloned and sequenced as previously described (Xia et al., 2008).

To evaluate the microbial ecology dynamics at different sampling times, the diversity index (Shannon-Weaver index, *H'*) and species richness (*d*) were calculated from the DGGE band profiles. Finally, cluster analysis and dendrogram generation were conducted using NTSYS-PC-2.10 (Exeter Software, USA) to evaluate the similarities in bacterial communities among DGGE patterns.

### 2.6. 16S rRNA gene-cloning and phylogenetic analysis

Clone libraries of 16S rRNA genes were constructed for DNA extracts obtained from biofilm samples collected on day 30, 70, and 102. Nearly complete 16S rRNA gene fragments were amplified in triplicate with primers 27F and 1492R using the PCR conditions described above (Xu et al., 2015). The PCR products were then purified with a QIA-quick PCR purification Kit (Qiagen, USA), after which they were inserted into the pTG19-T cloning vector using a TA Cloning Kit for Sequencing according to the manufacturer's instructions (Generay Co., Shanghai, China). Positive clones were identified by PCR amplification with the M13 primer set (Duan et al., 2013). For each biofilm sample, 100 positive clones were selected for sequencing. The average size of the aligned high-quality sequences was 700–800 bp, and all of the sequences were classified by finding their full-length matches in the NCBI GenBank database. The 16S rRNA gene sequences from this study have been deposited in the NCBI GenBank database under accession numbers JN125255–JN125354, JN125557–JN125656, and JN125757–JN125856.

For phylogenetic analysis, operational taxonomic units (OTUs) were defined as groups by setting a cutoff of 97% sequence similarity. Multiple alignments of the test and reference sequences were conducted using the Clustal-X software. A phylogenetic tree was then constructed by the neighbor-joining algorithm using the Mega 4.0 software with bootstrapping (1000 replicates).

## 3. Results and discussion

### 3.1. MBfR performance

The MBfR performance for the treatment of nitrate, sulfate, and *p*-CNB has previously been reported in detail as shown in Fig. S1 of the supporting information (Xia et al., 2011). In the first few days of the operation, the influent concentrations were only 10 mg NO<sub>3</sub><sup>-</sup>-N/L and 55 mg SO<sub>4</sub><sup>2-</sup>/L when H<sub>2</sub> was applied at 0.04 MPa. On day 30, *p*-CNB was added to the influent at 2 mg/L. Simultaneous biodegradation of nitrate, sulfate, and *p*-CNB occurred in the reactor when H<sub>2</sub> was used as

the electron donor, which was accompanied by different reduced products in the effluent. Next, 100 µg/L of *p*-CAN was detected in the effluent on day 33 (3 days after *p*-CNB addition). *p*-CAN began to be reduced to aniline (dechlorination) on day 44, or 14 days after *p*-CNB addition. A faster reduction of *p*-CNB to aniline (97 µg/L of *p*-CNB, or 4.9% residual) was evident by day 70, corresponding to 253 µg/L of effluent aniline concentration (Fig. S1). The reduced products, *p*-CAN and aniline, were detected in the effluent during the experiment, indicating that nitro-reduction of *p*-CNB and reductive dechlorination of *p*-CAN occurred in the biofilm. The H<sub>2</sub> pressure was increased to 0.05 MPa to enhance nitrate, sulfate and *p*-CNB reduction on day 71. Reduction of *p*-CNB to aniline increased continually to day 86, when the maximum aniline concentration of 460 µg/L was obtained. On day 87, the influent *p*-CNB concentration was increased to 5 mg/L with a loading of 0.145 g *p*-CNB/m<sup>2</sup>·d. The total quantity of *p*-CNB reduced was greatly enhanced (*p*-CNB flux increased from 0.055 g/m<sup>2</sup>·d to 0.097 g/m<sup>2</sup>·d), but the removal percentage of *p*-CNB decreased to 63.6%.

Table 1 presents a summary results of three steady states (Phases 1, 2, and 3) of the experiment. The dominant variations between phases were *p*-CNB addition and its concentration in influent, and H<sub>2</sub> pressure. During Phase 1, the nitrate and sulfate removal percentages were 80.9% and 10.9% with the removal fluxes of 0.233 g N/m<sup>2</sup>·d and 0.262 g SO<sub>4</sub><sup>2-</sup>/m<sup>2</sup>·d, respectively, and the influent nitrate and sulfate concentrations were 10 mg N/L and 55 mg SO<sub>4</sub><sup>2-</sup>/L. On day 31, *p*-CNB was added into the influent at 2 mg/L while the H<sub>2</sub> pressure was maintained at 0.04 MPa. On day 71, the H<sub>2</sub> pressure and *p*-CNB in the influent increased to 0.05 MPa and 5 mg/L, respectively. Increasing the H<sub>2</sub> pressure significantly enhanced sulfate reduction, resulting in a higher sulfate flux of 0.640 g/m<sup>2</sup>·d (effluent concentration of 33 mg/L) for the same sulfate influent concentration. During MBfR operation, the *p*-CNB fluxes ranged from 0.055 to 0.097 g/m<sup>2</sup>·d. At a *p*-CNB flux of 0.097 g/m<sup>2</sup>·d, the MBfR had an effluent *p*-CNB concentration of 1.82 mg/L and 63.6% *p*-CNB removal with H<sub>2</sub> at 0.05 MPa. As shown in Table 1, nitrate reduction was the greatest consumer of electrons (59.9%–79.2%), which was followed by sulfate reduction (20.8%–36.7%), and then reduction of *p*-CNB (2.5%–3.4%). When compared with *p*-CNB biodegradation, the removal of nitrate and sulfate was better, indicating that the total demand for H<sub>2</sub> was largely controlled by nitrate and sulfate reduction. Additionally, when substrate diffusion was restricted in a thick biofilm, the reaction kinetic was usually close to a half order (Rittmann and McCarty, 2001), which means that increasing *p*-CNB concentration cannot lead to a linear increase in *p*-CNB flux. Therefore, increasing the concentration of *p*-CNB and H<sub>2</sub> pressure did not improve the removal percentage of *p*-CNB. The utilization of H<sub>2</sub> in the three steady states of the MBfR is summarized in Table 1. During MBR operation (Phase 1 to Phase 3), effluent H<sub>2</sub> concentration decreased from 351 µg/L to 87 µg/L, and H<sub>2</sub> flux increased from 0.097 g/m<sup>2</sup> d to 0.143 g/m<sup>2</sup> d, revealing that the consumption of H<sub>2</sub> was increasing. Although the maximum H<sub>2</sub> utilization efficiency was nearly 100%, H<sub>2</sub> availability was still sufficient for the reactor.

### 3.2. DGGE fingerprint

To compare the dynamic response of the microbial ecology for *p*-CNB biodegradation and follow the temporal fluctuations in the bacterial community in the biofilm of the reactor, the PCR-based DGGE fingerprint was employed (Fig. 2). Cluster analysis of general microbial ecology in the biofilm revealed obvious variations in the bacterial community between inoculated bacteria and biofilms. The similarities between inoculated bacteria and the biofilm of Phases 1, 2 and 3 were 0.44, 0.48, and 0.48, respectively, indicating that the influent composition played the primary role in dynamic evolution of the microbial ecology in the biofilm. The microbial ecology in the biofilm of Phase 2 showed a high similarity (0.68) to that of Phase 3, but only 0.60 similarity to that of Phase 1 under similar HRT, influent nitrate and influent sulfate. Consequently, addition of *p*-CNB as an electron acceptor was a

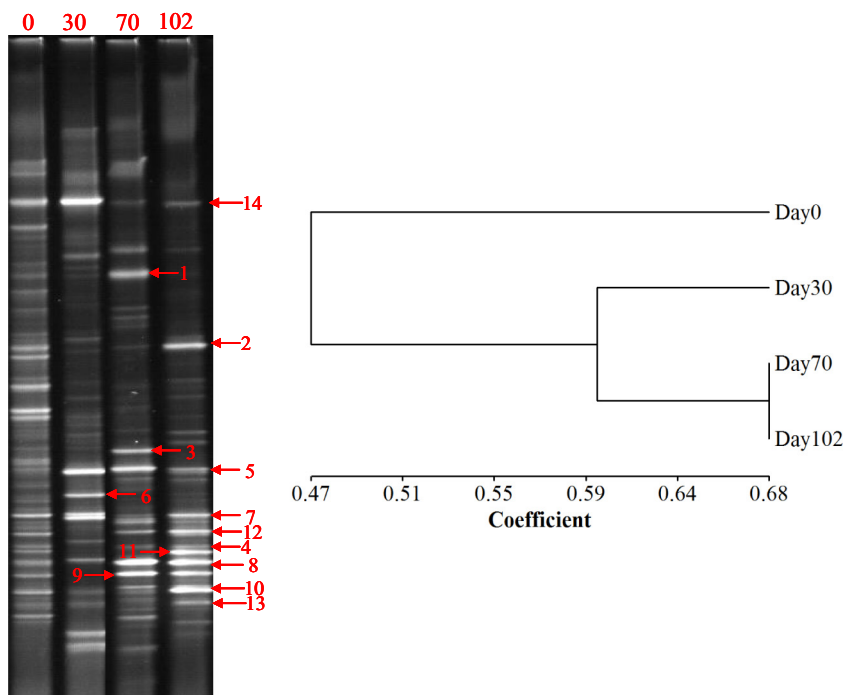


**Fig. 2.** DGGE profile and clustering analysis of general bacteria communities under different operational conditions. Day 0, Day 30, Day 70, and Day 102 are the days inoculated bacteria and biofilm samples (Phases 1, 2, and 3, respectively) were collected.

critical factor to the microbial ecology dynamic of MBfR biofilm. Zhou et al. (2014) and Ontiveros-Valencia et al. (2017) showed that electron acceptor compositional changes were the key factor that shaped the microbial community in U(VI) reducing MBfRs, suggesting that a dynamic response of the biofilm community structure to the presence of *p*-CNB in the present study.

The DGGE profile also revealed the dynamic response of microbial ecology during *p*-CNB biodegradation (Fig. 2). Specifically, bands 1, 2, 3, 6, and 11, which appeared in inoculated bacteria, disappeared or became brighter during the three phases. However, bands 5, 7, 8, 10, and 14 remained consistent throughout the operation, although their intensity varied in different phases. Table 2 further shows the bacterial diversity based on the Shannon-Weaver index ( $H'$ ) and species richness ( $d$ ) of microbial communities at different phases. The  $H'$  values of inoculated bacteria and biofilms collected from Phases 1, 2, and 3 were 3.20, 2.57, 2.49, and 2.49, respectively, indicating that the bacterial diversity of biofilm microbial ecology gradually decreased with changes in operational conditions, especially *p*-CNB concentration. Chen and Lapara (2006) reported that the composition of influent would obviously force the microbial ecology dynamic. The species richness gradually decreased from 54.8 (inoculated bacteria) to 24.9 (Phase 3) in the present study, indicating that microbial ecology evolved dynamically. Previous studies (Miao et al., 2017; Zhou et al., 2016) reported that enhanced microbial ecology dynamics provided better bacterial protection and more stable reactor performance, suggesting that the evolution of microbial ecology in the biofilm observed in the present study was the dynamic response for *p*-CNB in the reactor. The influent *p*-CNB concentration

increased from 2.0 mg/L (Phase 2) to 5.0 mg/L (Phase 3), while the  $H_2$  pressure increased from 0.04 MPa to 0.05 MPa. Nevertheless, the  $H'$  value of Phase 2 was similar to that of Phase 3. These findings indicate that the increase in influent *p*-CNB concentration and  $H_2$  pressure did not significantly change the bacterial diversity. Therefore, we can speculate that the addition of influent *p*-CNB leads to a more advantageous effect on the biofilm microbial community than variations in other operational conditions, such as *p*-CNB loading and  $H_2$  pressure.

Phylogenetic analysis demonstrated that most of the dominant species (78%) were *Proteobacteria*, followed by *Firmicutes* and *Bacteroidetes* (Fig. 3). In addition, the denitrifying bacteria *Thiobacillus denitrificans* (band 5), *Pseudomonas* sp. (band 8), and *Dechloromonas* sp. (band 14) were identified, which was attributed to the consistent denitrification in the biofilm under all of the conditions. The sulfate reducing bacteria, *Desulfovibrio*, was also detected in the biofilm (band 11) (Liu and Peck, 1981), which explains the higher sulfate reduction efficiency during Phase 3. Additionally, *Comamonas* (band 2) and *Pseudomonas* (band 8) were detected in all of the samples, indicating that they could play a very important role in the biodegradation of chlorinated aromatic compounds (Bergeron et al., 1994). *Hydrogenophilaceae* bacterium (Band 10) and *Hydrogenophaga* (Band 13) preferentially lived as the dominant species when hydrogen was present, indicating that they might be involved in the removal of electron acceptors.

### 3.3. Analysis of 16S rRNA clone library

Three 16S rRNA clone libraries were constructed to identify potentially dominant species in the biofilm during each phase. Each biofilm sample included about 100 randomly selected positive clones that were classified into different OTUs based on 97% sequence similarity. For the membrane biofilms of Phase 1, 2 and 3, the clones were classified into 40, 43, and 46 OTUs, respectively. Phylogenetic trees of the biofilms of Phase 1, 2, and 3 are shown in Figs. S2, S3 and S4 (Supporting information), respectively.

**Table 2**  
Bacterial diversity and species richness of microbial communities in biofilm.

|      | Inoculated bacteria | Phase 1 | Phase 2 | Phase 3 |
|------|---------------------|---------|---------|---------|
| $H'$ | 3.20                | 2.57    | 2.49    | 2.49    |
| $d$  | 54.8                | 39.9    | 34.9    | 24.9    |

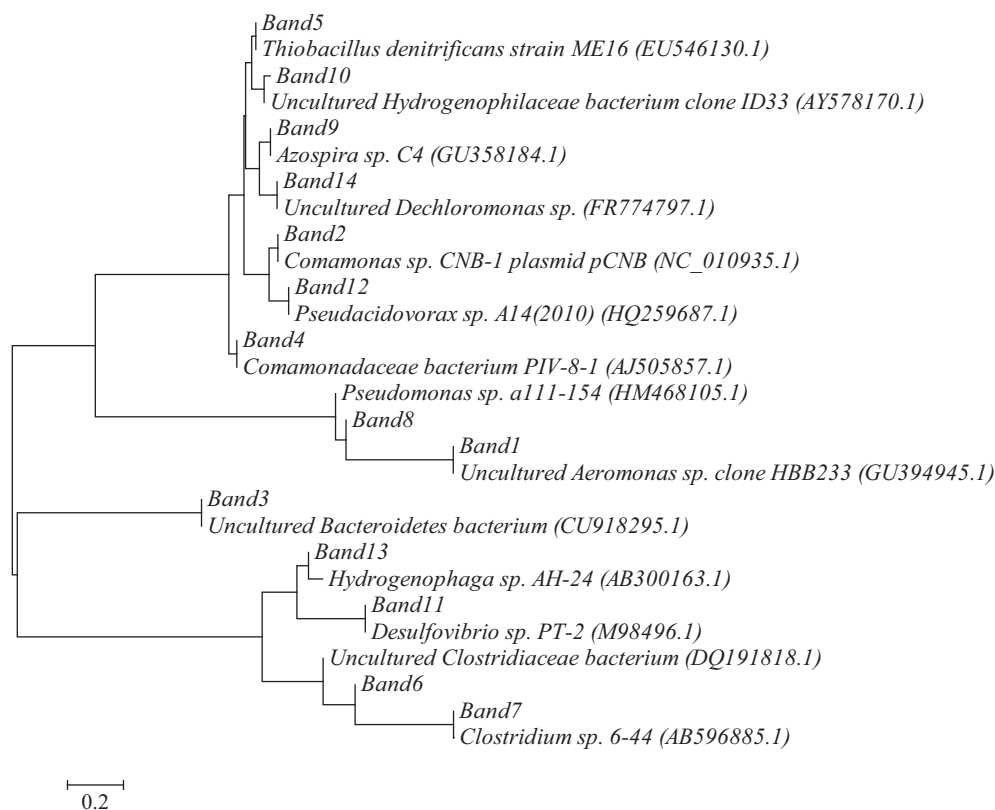


Fig. 3. Phylogenetic tree of bacterial sequences from DGGE bands.

Fig. 4 shows the taxonomic breakdown at the bacterial class level for all three phases. The bacterial communities of biofilm in each phase all showed complex dynamics, consisting of at least seven bacterial classes. *Betaproteobacteria*, *Gammaproteobacteria*, *Planctomycetacia*, *Deltaproteobacteria*, and *Alphaproteobacteria* were the dominant sequences in all biofilm samples. Moreover, *Betaproteobacteria* was the dominant bacteria throughout the MBfR operation, increasing with *p*-CNB biodegradation from 69.0% (Phase 1) to 77.0% (Phase 3). Additionally, *Gammaproteobacteria* showed rapid growth with *p*-CNB biodegradation, while *Planctomycetacia* was obviously inhibited during MBfR operation. The relative abundances of *Deltaproteobacteria* were also markedly higher at Phase 3, when there were higher rates of sulfate reduction. As shown in Table 3, *Betaproteobacteria*, *Gammaproteobacteria*, *Alphaproteobacteria*, and *Deltaproteobacteria* are the dominant

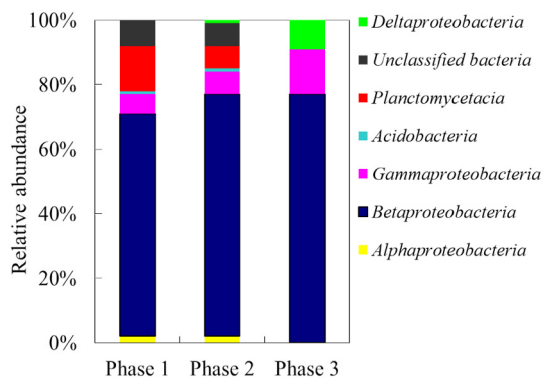


Fig. 4. Taxonomic breakdown (at the class level) of sequences from three biofilms. The relative abundance of a class within a microbial community was defined as the number of sequences affiliated with that class divided by the total number of sequences in that biofilm.

species in various autohydrogenotrophic biofilms used for treatment of different pollutants (Chung et al., 2008; Lai et al., 2014; Van Ginkel et al., 2010; Zhang et al., 2009; Zhao et al., 2013). These findings indicate that *Proteobacteria* play a significant role in the microbial ecology of autohydrogenotrophic biofilms for pollutants biodegradation, which is consistent with the *Proteobacteria* dynamics observed in the present study, suggesting that *Proteobacteria* is involved in the biodegradation of *p*-CNB. Consequently, the increase in *Proteobacteria* in biofilm was the dominant dynamic response of microbial ecology to *p*-CNB biodegradation during MBfR operation.

Fig. 5 shows further species analysis of the biofilm microbial community during *p*-CNB biodegradation. The relative abundances of dominant species (*Thiobacillus*, *Dechloromonas*, *Azospira*, *Thauera*, *Pseudomonas*, and *Desulfovibrio*) markedly increased with MBfR operation, indicating that these strongly enriched species were associated with the removal of electron acceptors. *Thiobacillus*, *Dechloromonas*, and *Desulfovibrio* have been reported as common nitrate and/or sulfate biodegradation bacteria. Moreover, the relative abundance of SRB *Desulfovibrio* (*Deltaproteobacteria*) increased from undetectable at Phase 1 to 7.2% at Phase 3, which agrees with the increasing removal of sulfate reduction (from 0.262 g/m<sup>2</sup>·d to 0.640 g/m<sup>2</sup>·d) in this reactor. Also of note, other nitrate and/or sulfate biodegradation bacteria, such as *Ideonella* and *Variovorax*, gradually decreased with *p*-CNB biodegradation. Both *Ideonella* and *Variovorax* are aerobic bacteria with heterotrophic metabolism (Bernner et al., 2005); thus, the relative percentage of these bacteria gradually decreased as the operating time of the reactor because of the anaerobic conditions. These results indicate long-term operation of the MBfR caused obvious effects on nitrate and sulfate biodegradation and the dynamic evolution of microbial ecology in biofilm. Finally, the abundance of nitrate and/or sulfate-reducing bacteria, such as *Thiobacillus*, *Dechloromonas*, *Azospira*, *Thauera*, *Pseudomonas*, and *Desulfovibrio*, increased significantly as H<sub>2</sub> pressure increased from 0.04 MPa (Phase 2) to 0.05 MPa (Phase 3), which was



#### 4. Conclusion

This study assessed the dynamic response of biofilm microbial ecology to *p*-CNB biodegradation in the MBfR. During operation, denitrification and sulfate reduction competed more strongly for H<sub>2</sub> than *p*-CNB reduction. The results of DGGE showed that the addition of *p*-CNB as an electron acceptor was a critical factor to the microbial ecology dynamics of MBfR biofilm. The presence of *p*-CNB had a more advantageous effect on the biofilm microbial community than increases in *p*-CNB loading and H<sub>2</sub> pressure. Clone library analysis showed that *Proteobacteria* are partially involved in *p*-CNB biodegradation of the MBfR, and that *Pseudomonas* sp. played a significant role in *p*-CNB biotransformation. Sufficient H<sub>2</sub> availability had a long-lasting effect on the microbial community structure that led to active nitrate, sulfate, and *p*-CNB reduction.

#### Acknowledgements

This work was supported by the Natural Science Foundation of China (51708362, 51768012, and 51678422), Guangxi Natural Science Foundation (2016GXNSFAA380204 and 2016GXNSFBA380207), State Key Laboratory of Pollution Control and Resource Reuse Foundation (PCRRF17025), and National Key Research and Development Program of China (2017YFC0403403). We would like to thank LetPub ([www.letpub.com](http://www.letpub.com)) for providing linguistic assistance during the preparation of this manuscript.

#### Appendix A. Supplementary data

Supplementary data to this article can be found online at <https://doi.org/10.1016/j.scitotenv.2018.06.245>.

#### References

- Aydin, E., Sahin, M., Taskan, E., Hasar, H., Erdem, M., 2016. Chlortetracycline removal by using hydrogen based membrane biofilm reactor. *J. Hazard. Mater.* 320, 88–95.
- Bergeron, J., Ahmad, D., Barriault, D., Larose, A., Sylvestre, M., Powlowski, J., 1994. Identification and mapping of the gene translation products involved in the first steps of the *Comamonas testosteroni* B-356 biphenyl/chlorobiphenyl biodegradation pathway. *Can. J. Microbiol.* 40, 743–753.
- Bernner, D.J., Krieg, N.R., Staley, J.T., 2005. *Bergey's manual of systematic bacteriology*. (2nd edition). Vol. Two: The Proteobacteria. East Lansing, MI, USA.
- Chen, R., Lapara, T.M., 2006. Aerobic biological treatment of low-strength synthetic wastewater in membrane-coupled bioreactors: the structure and function of bacterial enrichment cultures as the net growth rate approaches zero. *Microb. Ecol.* 51, 99–108.
- Chen, P., Li, J., Li, Q.X., Wang, Y., Li, S., Ren, T., Wang, L., 2012. Simultaneous heterotrophic nitrification and aerobic denitrification by bacterium *Rhodococcus* sp. CPZ24. *Bioresour. Technol.* 116 (13), 266–270.
- Chen, X.M., Liu, Y.W., Peng, L., Ni, B.J., 2017. Perchlorate, nitrate, and sulfate reduction in hydrogen-based membrane biofilm reactor: model-based evaluation. *Chem. Eng. J.* 316, 82–90.
- Chung, J., Nerenberg, R., Rittmann, B.E., 2006. Bio-reduction of soluble chromate using a hydrogen-based membrane biofilm reactor. *Water Res.* 40, 1634–1642.
- Chung, J., Ahn, C.H., Chen, Z., Rittmann, B.E., 2008. Bio-reduction of N-nitrosodimethylamine (NDMA) using a hydrogen-based membrane biofilm reactor. *Chemosphere* 70, 516–520.
- Duan, L., Song, Y.H., Xia, S.Q., Hermanowicz, S.W., 2013. Characterization of nitrifying microbial community in a submerged membrane bioreactor at short solids retention times. *Bioresour. Technol.* 149, 200–207.
- Hong, S.K., Anestis, D.K., Ball, J.G., Valentovic, M.A., Rankin, G.O., 2002. In vitro nephrotoxicity induced by chloronitrobenzenes in renal cortical slices from Fischer 344 rats. *Toxicol. Lett.* 129, 133–141.
- Huang, B.B., Qian, W.T., Yu, C.X., Wang, T., Zeng, G.M., Lei, C., 2016. Effective catalytic hydrodechlorination of *o*-, *p*- and *m*-chloronitrobenzene over Ni/Fe nanoparticles: effects of experimental parameter and molecule structure on the reduction kinetics and mechanisms. *Chem. Eng. J.* 306, 607–618.
- Lai, C.Y., Yang, X.E., Tang, Y.N., Rittmann, B.E., Zhao, H.P., 2014. Nitrate shaped the selenate-reducing microbial community in a hydrogen-based biofilm reactor. *Environ. Sci. Technol.* 48, 3395–3402.
- Le, C., Liang, J.Q., Wu, J.H., Li, P., Wang, X.D., Zhu, N.W., et al., 2011a. Effective degradation of para-chloronitrobenzene through a sequential treatment using zero-valent iron reduction and Fenton oxidation. *Water Sci. Technol.* 64, 2126–2131.
- Le, C., Wu, J.H., Deng, S.B., Li, P., Wang, X.D., Zhu, N.W., et al., 2011b. Effects of common dissolved anions on the reduction of para-chloronitrobenzene by zero-valent iron in groundwater. *Water Sci. Technol.* 63, 1485–1490.
- Li, H.X., Zhang, Z.Q., Xu, X.Y., Liang, J., Xia, S.Q., 2014. Bioreduction of para-chloronitrobenzene in a hydrogen-based hollow-fiber membrane biofilm reactor: effects of nitrate and sulfate. *Biodegradation* 25, 205–215.
- Liu, C.L., Peck, H.D., 1981. Comparative bioenergetics of sulfate reduction in *Desulfovibrio* and *Desulfotomaculum* spp. *J. Bacteriol.* 145, 966–973.
- Matsumoto, M., Aiso, S., Senoh, H., Yamazaki, K., Arito, H., Nagano, K., et al., 2006. Carcinogenicity and chronic toxicity of para-chloronitrobenzene in rats and mice by two-year feeding. *J. Environ. Pathol. Toxicol. Oncol.* 25, 571–584.
- Miao, L.Z., Wang, C., Hou, J., Wang, P.F., Ao, Y.H., Li, Y., et al., 2017. Response of wastewater biofilm to CuO nanoparticle exposure in terms of extracellular polymeric substances and microbial community structure. *Sci. Total Environ.* 579, 588–597.
- Niu, G.L., Zhang, J.J., Zhao, S., Liu, H., Boon, N., Zhou, N.Y., 2009. Bioaugmentation of a 4-chloronitrobenzene contaminated soil with *Pseudomonas putida* ZWL73. *Environ. Pollut.* 157, 763–771.
- Ontiveros-Valencia, A., Zhou, C., Ilhan, Z.E., Cyr, L.C.D.S., Krajmalnik-Brown, R., Rittmann, B.E., 2017. Total electron acceptor loading and composition affect hexavalent uranium reduction and microbial community structure in a membrane biofilm reactor. *Water Res.* 125, 341–349.
- Park, H.S., Lim, S.J., Chang, Y.K., Livingston, A.G., Kim, H.S., 1999. Degradation of chloronitrobenzenes by a coculture of *Pseudomonas putida* and a *Rhodococcus* sp. *App. Environ. Microb.* 65 (3), 1083–1091.
- Rittmann, B.E., McCarty, P.L., 2001. *Environmental biotechnology: principles and applications*. McGraw-Hill Book Co., New York, USA.
- Su, W., Zhang, L., Li, D., Zhan, G., Qian, J., Yong, T., 2012. Dissimilatory nitrate reduction by *Pseudomonas alcaliphila* with an electrode as the sole electron donor. *Biotechnol. Bioeng.* 109 (11), 2904–2910.
- Van Ginckel, S.W., Lamendella, R., Kovacic, W.P., Domingo, J.W.S., Rittmann, B.E., 2010. Microbial community structure during nitrate and perchlorate reduction in ion-exchange brine using the hydrogen-based membrane biofilm reactor (MBfR). *Bioresour. Technol.* 101, 3747–3750.
- Wu, J.F., Jiang, C.Y., Wang, B.J., Ma, Y.F., Liu, Z.P., Liu, S.J., 2006. Novel partial reductive pathway for 4-chloronitrobenzene and nitrobenzene degradation in *Comamonas* sp strain CNB-1. *App. Environ. Microb.* 72 (3), 1759–1765.
- Wu, H.Z., Wei, C.H., Wang, Y.Q., He, Q.C., Liang, S.Z., 2009. Degradation of *o*-chloronitrobenzene as the sole carbon and nitrogen sources by *Pseudomonas putida* OCNB-1. *J. Environ. Sci.* 21, 89–95.
- Wu, Y., Shukal, S., Mukherjee, M., Cao, B., 2015. Involvement in denitrification is beneficial to the biofilm lifestyle of *Comamonas testosteroni*: A mechanistic study and its environmental implications. *Environ. Sci. Technol.* 49 (19), 11551–11559.
- Wu, Y.F., Gan, L., Zhang, S.P., Jiang, B.C., Song, H.O., Li, W.T., et al., 2017. Enhanced electrocatalytic dechlorination of para-chloronitrobenzene based on Ni/Pd foam electrode. *Chem. Eng. J.* 316, 146–153.
- Xia, S.Q., Guo, J.F., Wang, R.C., 2008. Performance of a pilot-scale submerged membrane bioreactor (MBR) in treating bathing wastewater. *Bioresour. Technol.* 99, 6834–6843.
- Xia, S.Q., Li, J.X., Wang, R.C., Li, J.Y., Zhang, Z.Q., 2010. Tracking composition and dynamics of nitrification and denitrification microbial community in a biofilm reactor by PCR-DGGE and combining FISH with flow cytometry. *Biochem. Eng. J.* 49, 370–378.
- Xia, S.Q., Li, H.X., Zhang, Z.Q., Zhang, Y.H., Yang, X., Jia, R.Y., et al., 2011. Bioreduction of para-chloronitrobenzene in drinking water using a continuous stirred hydrogen-based hollow fiber membrane biofilm reactor. *J. Hazard. Mater.* 192, 593–598.
- Xia, S.Q., Xu, X.Y., Zhou, C., Wang, C.H., Zhou, L.J., Rittmann, B.E., 2016. Direct delivery of CO<sub>2</sub> into a hydrogen-based membrane biofilm reactor and model development. *Chem. Eng. J.* 290, 154–160.
- Xiao, Y., Wu, J.F., Liu, H., Wang, S.J., Liu, S.J., Zhou, N.Y., 2006. Characterization of genes involved in the initial reactions of 4-chloronitrobenzene degradation in *Pseudomonas putida* ZWL73. *Appl. Microbiol. Biotechnol.* 73, 166–171.
- Xu, X.Y., Xia, S.Q., Zhou, L.J., Zhang, Z.Q., Rittmann, B.E., 2015. Bioreduction of vanadium (V) in groundwater by autohydrogenotrophic bacteria: mechanisms and microorganisms. *J. Environ. Sci.* 30, 122–128.
- Zhang, Y.H., Zhong, F.H., Xia, S.Q., Wang, X.J., Li, J.X., 2009. Autohydrogenotrophic denitrification of drinking water using a polyvinyl chloride hollow fiber membrane biofilm reactor. *J. Hazard. Mater.* 170, 203–209.
- Zhang, H., Ziv-el, M., Rittmann, B.E., Krajmalnik-Brown, R., 2010. Effect of dechlorination and sulfate reduction on the microbial community structure in denitrifying membrane-biofilm reactors. *Environ. Sci. Technol.* 44, 5159–5164.
- Zhang, L.J., Wang, X., Jiao, Y.Y., Chen, X., Zhou, L.Y., Guo, K., et al., 2013. Biodegradation of 4-chloronitrobenzene by biochemical cooperation between *Sphingomonas* sp. strain CNB3 and *Burkholderia* sp. strain CAN6 isolated from activated sludge. *Chemosphere* 91, 1243–1249.
- Zhang, Y., Chen, J.X., Wen, L.L., Tang, Y.N., Zhao, H.P., 2016. Effects of salinity on simultaneous reduction of perchlorate and nitrate in a methane-based membrane biofilm reactor. *Environ. Sci. Pollut. Res.* 23, 24248–24255.
- Zhao, H.P., Ilhan, Z.E., Ontiveros-Valencia, A., Tang, Y.N., Rittmann, B.E., Krajmalnik-Brown, R., 2013. Effects of multiple electron acceptors on microbial interactions in a hydrogen-based biofilm. *Environ. Sci. Technol.* 47, 7396–7403.
- Zhou, C., Ontiveros-Valencia, A., Cyr, L.C.D.S., Zevin, A.S., Carey, S.E., Krajmalnik-Brown, R., Rittmann, B.E., 2014. Uranium removal and microbial community in a H<sub>2</sub>-based membrane biofilm reactor. *Water Res.* 64 (22), 255–264.
- Zhou, L.J., Zhao, M., Feng, L., Wang, X., Xu, X.Y., Xia, S.Q., 2016. Performance and bacterial community structure of an anoxic/oxic membrane bioreactor treating anaerobically digested piggyery wastewater. *Desalin. Water Treat.* 57, 28581–28591.
- Zhu, L., Lin, H.Z., Qi, J.Q., Xu, X.Y., Qi, H.Y., 2012. Effect of H<sub>2</sub> on reductive transformation of *p*-CINB in a combined ZVI-anaerobic sludge system. *Water Res.* 46, 6291–6299.